Available online at www.sciencedirect.com

ScienceDirect

International Journal of Solids and Structures 45 (2008) 1244–1263

INTERNATIONAL JOURNAL OF SOLIDS AND STRUCTURES

www.elsevier.com/locate/ijsolstr

Calibrating a J2 plasticity material model using a 2D inverse finite element procedure

Hasan Charkas [a], Hayder Rasheed [b,*], Yacoub Najjar [b]

[a] *Structural & Fracture Mechanics Unit, AREVA NP Inc., Lynchburg, VA 24501, USA*
[b] *Department of Civil Engineering, Kansas State University, Manhattan, KS 66506, USA*

Received 18 May 2007; received in revised form 13 July 2007
Available online 4 November 2007

Abstract

Material models are the key ingredients to accurately capture the global mechanical response of structural systems. The use of finite element analysis has proven to be effective in simulating nonlinear engineering applications. However, the choice of the appropriate material model plays a big role in the value of the numerical predictions. Such models are not expected to exactly reproduce global experimental response in all cases. Alternatively, the measured global response at specific domain or surface points can be used to guide the nonlinear analysis to successively extract a representative material model. By selecting an initial set of stress–strain data points, the load–displacement response at the monitoring points is computed in a forward incremental analysis without iterations. This analysis retains the stresses at the integration points. The corresponding strains are not accurate since the computed displacements are not anticipated to match the measured displacements at the monitoring points. Therefore, a corrective incremental displacement analysis is performed at the same load steps to adjust for displacements and strains everywhere by matching the measured displacements at the monitoring points. The stress–strain vectors at the most highly stressed integration point are found to establish an improved material model. This model is used within a multi-pass incremental nonlinear finite element analysis until the discrepancy between the measured and the predicted structural response at the monitoring points vanishes. The J2 flow theory of plasticity is used as a constitutive framework to build the tangent elastic–plastic matrices. The applicability of the proposed approach is demonstrated by solving 2D inverse continuum problems. The comparisons presented support the effectiveness of the proposed approach in accurately calibrating the J2 plasticity material model for such problems.

Keywords: Inverse problem; Finite element analysis; Nonlinear constitutive modeling; Plasticity

1. Introduction

Inverse techniques have been utilized in a wide range of engineering disciplines and applications (Sakurai, 1983; Gelin and Ghouati, 1995; Rikards et al., 2001; Li and Chen, 2000; Liu et al., 2002). These applications are related to the prediction of input excitation from structural response, damage detection by vibration

* Corresponding author. Tel.: +1 785 532 1589; fax: +1 785 532 7717.
E-mail address: hayder@ksu.edu (H. Rasheed).

0020-7683/$ - see front matter © 2007 Elsevier Ltd. All rights reserved.
doi:10.1016/j.ijsolstr.2007.09.033

techniques and material parameter identification from global structural measurements. The inverse techniques introduced in the literature to date use various averaging, interpolation or optimization tools ranging from the least squares and nonlinear programming, to minimize the difference between the numerical solution and experimental results, to neural networks, evolutionary computational models such as genetic algorithms and linguistic based methods such as fuzzy logic to fit the data. The utilization of such tools requires a considerable data storage, processing and computational effort.

The material identification approaches developed to formulate the inverse problem in earlier studies are either based on vibration/dynamic readings or on quasi-static displacement measurements. The approaches based on quasi-static displacement measurements are reviewed in this paper. Gelin and Ghouati (1995) proposed an inverse identification method to determine material parameters in metal forming. The method is based on optimization process, which is minimizing a nonlinear least squares function with respect to the parameters to be identified. The method was applied to identify the viscoplastic behavior of aluminum alloys using both plane strain and axisymmetric compression tests. In this study, it was necessary to evaluate the influence of material parameters variation on the calculated response. This was accomplished using a sensitivity analysis based on a direct differentiation method consistent with the finite element formulation. Markiewicz et al. (1998) presented an inverse approach that used experimental quasi-static and dynamic axial crushing of thin-walled square tubes to determine the constitutive model parameters. Lam et al. (1998) clarified *two* different requirements *for torsion and compression tests* to solve the problem of identifying constitutive parameters using an inverse computational method. They assumed the material behavior to be viscoplastic described by a power law constitutive equation. They showed that using a cost function based on a single set of load–displacement data (with a constant displacement rate) will not lead to determination of a unique set of parameters for torsion test while it is sufficient for plane strain and axisymmetric compression tests. Ghaboussi et al. (1998) used a combined neural network and finite element algorithm to inversely solve for the nonlinear in-plane shear material model of [±45 s] composite laminates. The ply normal stress–strain states were considered to assume a linear response. Since the ply shear response was uncoupled from normal stress–strain relationship, the algorithm was basically handling a uniaxial nonlinear stress–strain state. The neural network was used to average all stress–strain predictions in the mesh to produce a material model. In addition, they avoided formulating an explicit stiffness matrix by using conjugate gradient method to solve for displacement increments. Ohkami and Swoboda (1999) presented two procedures to identify the linear viscoelastic material parameters using observed displacements and/or tractions. They introduced the parameters in the finite element equations and solved for them using nonlinear least squares. One method uses the incremental constitutive relation for linear viscoelastic materials. This method provides sufficiently accurate results but requires complicated formulations and extensive computing time. The second method is based on the elastic viscoelastic correspondence principle. This method is easier to implement. However, the accuracy of the results depends on the accuracy of the initial energy estimate. Shin and Pande (2000) presented another combined neural network and finite element algorithm to construct a linear neural network material model from global response. They built a constitutive matrix based on the derivatives of the neural network weights and averaged the coefficients of the matrix to achieve symmetry. Soh and Dong (2001) proposed an evolutionary program incorporated with finite elements for solving inverse problems. First, they assumed a trial value of the properties to calculate displacements based on these values. Then an improved genetic algorithm was used to solve the optimization process by minimizing the difference between the calculated and the measured values. Forestier et al. (2002) proposed an inverse model to estimate thermo-mechanical parameters from inhomogeneous mechanical tests. The method was based on comparison of data obtained from measurements with the results obtained from the direct model. The problem was formulated based on least square technique and the optimization was solved using Gauss–Newton algorithm. Furukawa et al. (2002) formulated a parameter identification procedure for inelastic constitutive models. They used a least square format to develop a stress error function minimized by a gradient-incorporated continuous evolutionary algorithm (GICEA). Measured stress–strain data were used to guide the inverse solution, which is different from the global response used in the present study. In another paper, Shin and Pande (2003) used the same methodology explained above to identify elastic constants of orthotropic materials with known principal material axes a priori. After constructing the constitutive matrix based on the derivatives of the neural network weights, the values in the matrix are compared to the conventional orthotropic elasticity matrix. Nayal and Rasheed (2006) developed an inverse

approach to extract model parameters simulating the homogenized tensile behavior of concrete. The formulation combined nonlinear numerical analysis, predefined material functions and global experimental response to develop the best model parameters in the case of concrete beams reinforced with steel and FRP bars.

The present proposed work is intended to develop a robust and efficient solution strategy to solve 2D inverse finite element problems without any need to a data averaging, interpolating or minimization techniques. By focusing on the constitutive response of the most highly stressed integration point, a unique set of adaptively improved stress–strain vectors can be obtained to extract the universal curve of the plasticity model from global structural response. Explicit formulation of the tangent stiffness matrix is presented using the J2 flow theory of plasticity as a framework to handle the multi-axial state of stress. Several examples are demonstrated and useful comparisons and conclusions are highlighted. It is important to note that the present algorithm is validated for monotonic loading only. Cyclic loading is beyond the scope of this work.

2. Formulation of the present approach

The present approach is intended to extract the nonlinear material response of 2D continuum metals. The measured load–displacement data at some monitoring points are provided as input to the inverse algorithm along with the geometry and applied loads. The present approach consists of two conjugate incremental analyses called stress-predictive and strain-predictive. In the stress-predictive analysis, the tangent stiffness matrix at each load increment, based on the current material model, is used to calculate the displacement increments without iterations:

$$\left\{\begin{array}{c}\Delta\mathbf{P}_{\mathrm{f}}\\ \Delta\mathbf{P}_{\mathrm{s}}\end{array}\right\}=\left[\begin{array}{cc}\mathbf{K}^{\mathrm{t}}_{\mathrm{ff}} & \mathbf{K}^{\mathrm{t}}_{\mathrm{fs}}\\ \mathbf{K}^{\mathrm{t}}_{\mathrm{sf}} & \mathbf{K}^{\mathrm{t}}_{\mathrm{ss}}\end{array}\right]\left\{\begin{array}{c}\Delta\mathbf{U}_{\mathrm{f}}\\ \Delta\mathbf{U}_{\mathrm{s}}\end{array}\right\}\Rightarrow\{\Delta\mathbf{U}_{\mathrm{f}}\}=\left\{\begin{array}{c}\Delta\mathbf{U}_{\mathrm{ro}}\\ \Delta\mathbf{U}_{\mathrm{rm}}\end{array}\right\}=\left[\mathbf{K}^{\mathrm{t}}_{\mathrm{ff}}\right]^{-1}\{\Delta\mathbf{P}_{\mathrm{f}}\} \tag{1}$$

where $\{\Delta\mathbf{U}_{\mathrm{f}}\}$ is the incremental vector of the free displacement degrees of freedom, $\{\Delta\mathbf{U}_{\mathrm{s}}\}$ corresponds to the suppressed displacement degrees of freedom, $\{\Delta\mathbf{U}_{\mathrm{rm}}\}$ is the incremental vector of the monitored degrees of freedom that are released in this analysis, $\{\Delta\mathbf{U}_{\mathrm{ro}}\}$ is the incremental vector of the rest of free degrees of freedom, $\{\Delta\mathbf{P}_{\mathrm{f}}\}$ is the vector of incremental applied forces and $\{\Delta\mathbf{P}_{\mathrm{s}}\}$ is the vector of incremental support reactions. This yields sets of stress–strain data at the integration points. The current displacements predicted at the monitoring points are not expected to match the measured displacements at these points for a partially improved material model, Fig. 1. Accordingly, the strains, computed in this analysis, are not expected to be accurate. On the other hand, the stresses calculated in this analysis are more consistent with the applied loads since the two are related only through the equilibrium equations. Therefore, this computational process is called stress-predictive analysis since only stresses are retained.

$$\Delta\boldsymbol{\varepsilon}_j=\mathbf{B}_j\Delta\mathbf{U}_{\mathrm{element}},\quad \Delta\boldsymbol{\sigma}_j=\mathbf{D}^{\mathrm{ep}}_{\mathrm{t}}\Delta\boldsymbol{\varepsilon}_j,\quad \boldsymbol{\sigma}^i_j=\boldsymbol{\sigma}^{i-1}_j+\Delta\boldsymbol{\sigma}_j \tag{2}$$

$$\mathbf{P}^i_{\mathrm{int}}=\int_{\mathrm{vol}}\mathbf{B}^{\mathrm{T}}_j\boldsymbol{\sigma}^i_j\,\mathrm{d}v \tag{3}$$

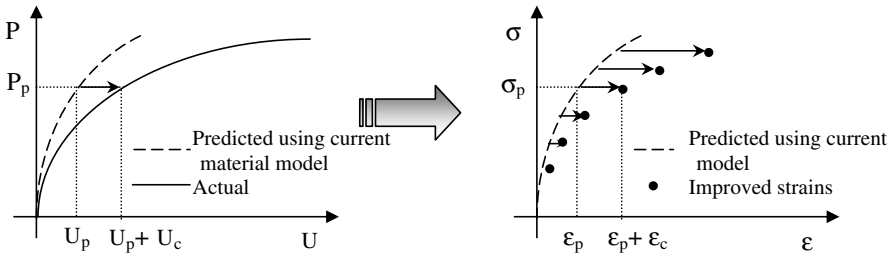

(a) Actual and predicted-corrected response at a monitoring point

(b) Predicted-adjusted strain at an integration point

Fig. 1. Displacement and strain correction guided by monitored point response.

where $\mathbf{P}_{\text{int}}^{i}$ is the internal force vector of load step i, $\mathbf{B}_j$ is the matrix relating strains to displacements at integration point j, $\mathbf{D}_{\text{t}}^{\text{ep}}$ is the tangent elastic–plastic constitutive matrix of the current material model, $\boldsymbol{\sigma}_j^i$ is the stress vector of the current load step i at an integration point j. In order to generate corresponding strains that are consistent with the actual displacements at the monitoring points, a conjugate analysis is performed with known prescribed displacements at the monitoring points, Fig. 1:

$$\begin{aligned}\{\Delta\mathbf{P}_{\text{f}}\} = \left[\mathbf{K}_{\text{ff}}^{\text{t}}\right]\{\Delta\mathbf{U}_{\text{f}}\} \Rightarrow \begin{Bmatrix}\Delta\mathbf{P}_{\text{r}} = 0\\ \Delta\mathbf{P}_{\text{m}}\end{Bmatrix} &= \begin{bmatrix}\mathbf{K}_{\text{rr}}^{\text{t}} & \mathbf{K}_{\text{rm}}^{\text{t}}\\ \mathbf{K}_{\text{mr}}^{\text{t}} & \mathbf{K}_{\text{mm}}^{\text{t}}\end{bmatrix}\begin{Bmatrix}\Delta\mathbf{U}_{\text{r}}\\ \Delta\mathbf{U}_{\text{m}} - \Delta\mathbf{U}_{\text{rm}}\end{Bmatrix}\\ \Rightarrow \{\Delta\mathbf{U}_{\text{r}}\} &= -[\mathbf{K}_{\text{rr}}^{\text{t}}]^{-1}\mathbf{K}_{\text{rm}}^{\text{t}}\{\Delta\mathbf{U}_{\text{m}} - \Delta\mathbf{U}_{\text{rm}}\}\end{aligned} \tag{4}$$

where $\{\Delta\mathbf{U}_{\text{m}}\}$ is the measured incremental vector of monitored degrees of freedom of that load step, $\{\Delta\mathbf{U}_{\text{m}} - \Delta\mathbf{U}_{\text{rm}}\}$ is the incremental displacement error vector at the monitored degrees of freedom and $\{\Delta\mathbf{U}_{\text{r}}\}$ is the incremental vector of released degrees of freedom due to the imposed incremental displacement error vector. The displacements from the two conjugate analyses are added together to obtain a displacement vector that is consistent with the actual measured displacements at the monitoring points:

$$\Delta\mathbf{U}_{\text{f}}^{\text{adj}} = \begin{Bmatrix}\Delta\mathbf{U}_{\text{ro}} + \Delta\mathbf{U}_{\text{r}}\\ \cancel{\Delta\mathbf{U}_{\text{rm}}} + \Delta\mathbf{U}_{\text{m}} - \cancel{\Delta\mathbf{U}_{\text{rm}}}\end{Bmatrix} \tag{5}$$

where $\{\Delta\mathbf{U}_{\text{f}}^{\text{adj}}\}$ is the adjusted incremental displacement vector of the load step in hand. The strains obtained from this vector are consistent with the measured displacements at the monitoring points. Accordingly, the second analysis is called strain-predictive analysis.

$$\Delta\boldsymbol{\varepsilon}_j = \mathbf{B}_j\Delta\mathbf{U}_{\text{element}}^{\text{adj}}, \quad \boldsymbol{\varepsilon}_j^i = \boldsymbol{\varepsilon}_j^{i-1} + \Delta\boldsymbol{\varepsilon}_j \tag{6}$$

where $\boldsymbol{\varepsilon}_j^i$ is the strain vector of the current load step i at the integration point of interest j, $\boldsymbol{\varepsilon}_j^{i-1}$ is the corresponding strain vector of the previous load step. It is relevant to establish that this approach is only applicable to quasi-static analysis at this stage.

It is worth mentioning here that the present procedure does not retain the improved stress–strain data of all integration points. Instead, it saves the stress–strain vectors computed at the most highly stressed integration point. The most highly stressed integration point is identified as the point of maximum J2-type effective stress based on initial linear analysis.

$$\sigma_{\text{e}} = \sqrt{3J_2} = \sqrt{\frac{3}{2}S_{ij}S_{ij}} \tag{7}$$

where J_2 is the second invariant of the deviatoric stress tensor, S_{ij} is a component of the deviatoric stress tensor.

The stress–strain sets, predicted after each dual analysis cycle, are expected to get closer to the actual material model. It has been observed, in this study, that the stress–corrected strain data set at the most highly stressed integration point provides the most accurate representation of an improved material model. This finding is further explained and justified below. Accordingly, this set of stress–strain vectors is retained and used as a unique material model without averaging with stress–strain data sets at the rest of integration points. This treatment requires minimal data storage and provides an explicit formulation of the material model.

3. Selecting the most highly stressed integration point

It is important to realize that the strain-predictive analysis imposes the displacement error of the monitoring points onto the entire domain as an added displacement effect. This causes a similar strain correction throughout the mesh regardless of the stress levels. Accordingly, any nonlinearity in the measured global response of the monitoring points will be similarly reflected on stress–strain values of all the integration points because of the nature of strain correction in the present algorithm. These integration points have different levels of stress for a certain load step. Therefore, the highly stressed integration points are the ones that should

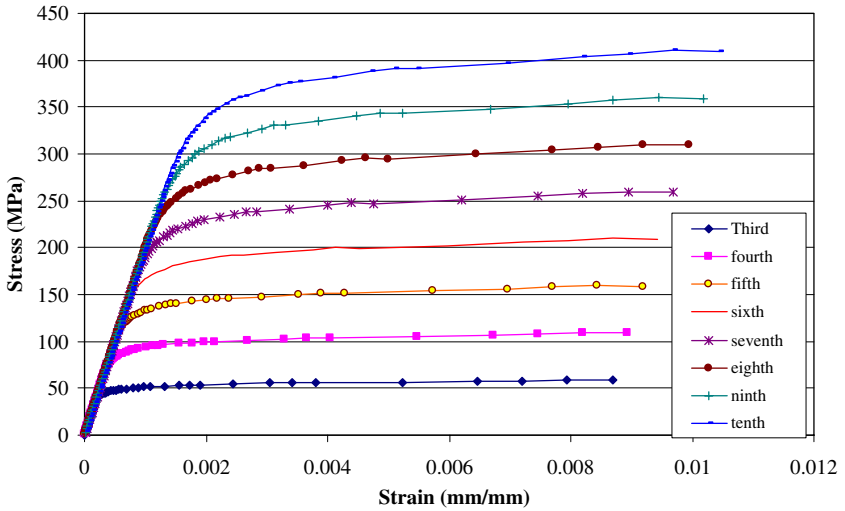

Fig. 2. Stress–strain predictions at different integration points of a simple structure after a complete analysis pass.

undergo the material nonlinearity reflected by the global response while the lightly stressed integration points are still undergoing linear behavior for a specific material model throughout the structure. Accordingly, the displacement correction yields more accurate stress–strain estimates at highly stressed integration points. To further clarify this finding, the stress–corrected strain data sets at different integration points of a simple mechanical model are plotted at the end of an analysis pass, Fig. 2. Fig. 2 shows that the predictions at all integration points exhibit yielding response at different stress levels. This yielding inflected by global response can only take place at the highly stressed integration points for a certain strain level. Therefore, selecting the data set from the most highly stressed integration point provides the most accurate interim prediction, the quality of which may be compromised when averaging with predictions at lower stress levels. It is important to note that the present study is limited to monotonic loading only. Careful examination of this concept is needed when unloading is treated.

4. Linear parameter identification

Capturing the linear material model parameters in the present approach depends only on using the first load increment where the material is truly elastic. The initially assumed E and v values are used to build the initial stiffness matrix that is needed to have estimates of displacements at the monitoring points. These displacements are not expected to match the actual displacements at the monitoring points for the first load increment since the stiffness matrix is developed from arbitrarily assumed material parameters. The stress-predictive and strain-predictive analyses are applied to generate improved stress–strain data at all integration points based on matching the load–displacement response at the monitoring points, Fig. 1. Only the stress–strain set at the most highly stressed integration point is retained and used to extract better estimates of the material parameters for the next analysis pass. The determination of improved elastic constants for isotropic materials is easily carried out using the improved stress–strain values. For example, the constitutive matrix in the case of 2D plane stress analysis is:

$$\begin{bmatrix}\sigma_{11}\\ \sigma_{22}\\ \sigma_{12}\end{bmatrix} = \begin{bmatrix}A & vA & 0\\ vA & A & 0\\ 0 & 0 & G\end{bmatrix}\begin{bmatrix}\varepsilon_{11}\\ \varepsilon_{22}\\ \gamma_{12}\end{bmatrix} \quad \text{where } A = \frac{E}{1-v^2} \tag{8}$$

The improved stress–strain data set at the most highly stressed integration point is known in the case of the inverse analysis. Solving the first two rows of Eq. (8) for v and A:

$$v = \frac{(\sigma_{22}\varepsilon_{11} - \sigma_{11}\varepsilon_{22})}{(\sigma_{11}\varepsilon_{11} - \sigma_{22}\varepsilon_{22})}, \quad A = \frac{\sigma_{11}}{\varepsilon_{11} + v\varepsilon_{22}} = \frac{E}{1 - v^2}$$
$$E = \frac{(1 - v^2)\sigma_{11}}{\varepsilon_{11} + v\varepsilon_{22}}, \quad G = \frac{E}{2(1 + v)} \tag{9}$$

The Poisson's ratio estimate needs to be in the range of 0–0.5. The prediction of v values outside this range would require repeating the inverse analysis with different initial parameter estimates or selecting better locations of monitoring points. This was not the case for the examples solved in this paper. The process of predicting improved elastic constants is repeated until the difference between the displacement at the monitoring points and the corresponding predicted displacement at the end of the stress-predictive analysis is less than a specified tolerance.

5. Nonlinear J2 model calibration

At the end of the identification of linear parameters, the algorithm is ready to inversely recover the entire nonlinear material model. Linear behavior is the best initial estimate in hand of the material model that could be provided to the inverse finite element procedure. Therefore, the stiffness matrix used in the first pass is linear for all load increments. The well-known J2 flow theory of plasticity with isotropic hardening is used as a constitutive framework to build the tangent elastic–plastic matrices. Accordingly, some of its standard formulas are invoked here to form the basis of the present formulation. The relationship between the increment in effective plastic strain and the incremental effective stress is below, see Fig. 3:

$$\mathrm{d}\varepsilon_{\mathrm{e}}^{\mathrm{p}} = \frac{\mathrm{d}\sigma_{\mathrm{e}}}{H} = \sqrt{\frac{2}{3}\mathrm{d}\boldsymbol{\varepsilon}^{\mathrm{p}}\mathrm{d}\boldsymbol{\varepsilon}^{\mathrm{p}}} \tag{10}$$

where $\mathrm{d}\varepsilon_{\mathrm{e}}^{\mathrm{p}}$ is the increment in effective plastic strain, σ_{e} is the effective stress defined in Eq. (7) and H is the hardening modulus. Based on the normality rule and continuity condition, the vector of incremental plastic strain ($\mathrm{d}\boldsymbol{\varepsilon}^{\mathrm{p}}$) is written as:

$$\mathrm{d}\boldsymbol{\varepsilon}^{\mathrm{p}} = \frac{1}{H}\left(\frac{\partial f}{\partial \boldsymbol{\sigma}} \cdot \partial\boldsymbol{\sigma}\right)\frac{\partial f}{\partial \boldsymbol{\sigma}} = \frac{9}{4}\frac{\mathbf{s} \cdot \mathrm{d}\boldsymbol{\sigma}}{H\sigma_{\mathrm{e}}^2}\mathbf{s} \tag{11}$$

Accordingly, the incremental constitutive relationship is expressed below, which may be easily inverted to yield the stress–strain expression:

$$\mathrm{d}\varepsilon_{ij} = \mathrm{d}\varepsilon_{ij}^{\mathrm{e}} + \mathrm{d}\varepsilon_{ij}^{\mathrm{p}} = \frac{1 + v}{E}\mathrm{d}\sigma_{ij} - \frac{v}{E}\mathrm{d}\sigma_{kk}\delta_{ij} + \frac{9s_{pq}\mathrm{d}\sigma_{pq}}{4H\sigma_{\mathrm{e}}^2}s_{ij} = C_{ijkl}^{\mathrm{ep}}\mathrm{d}\sigma_{kl} \tag{12}$$

$$\text{or} \quad \mathrm{d}\sigma_{ij} = D_{ijkl}^{\mathrm{ep}}\mathrm{d}\varepsilon_{kl} \tag{13}$$

where C_{ijkl}^{ep} is the component of the elastic–plastic compliance tensor and D_{ijkl}^{ep} is the corresponding component of the elastic–plastic constitutive tensor. In the present inverse approach, however, none of the parameters in

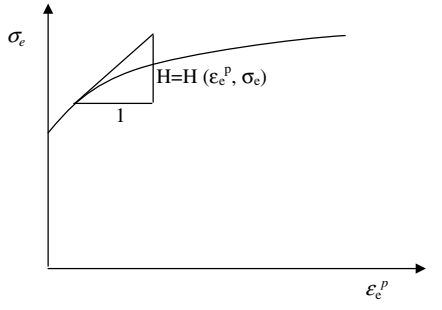

Fig. 3. Typical effective plastic strain–effective stress curve for nonlinear material.

Eq. (12) is known a priori and the main objective is to extract the correct J2 universal curve using global load–displacement response at specific monitoring points.

In the present approach, strain values that are deviating from linearity are considered to be plastic strains. The plastic strain vector, at the most highly stressed integration point, is found at the end of each strain-predictive analysis by subtracting strains obtained using the linear material properties from the total improved strain values:

$$\boldsymbol{\varepsilon}^{i\mathrm{p}}_{\text{int pt}} = \boldsymbol{\varepsilon}^{i}_{\text{int pt}} - \boldsymbol{\varepsilon}^{i\mathrm{e}}_{\text{int pt}} \tag{14}$$

where $\boldsymbol{\varepsilon}^{i\mathrm{p}}_{\text{int pt}}$ is the plastic strain vector of load step i at the most highly stressed integration point, which is used to build the effective plastic strain $\varepsilon^{i\mathrm{p}}_{\mathrm{e}}$, $\boldsymbol{\varepsilon}^{i}_{\text{int pt}}$ is the total strain vector of load step i at the most highly stressed integration point, after applying the strain-predictive analysis and $\boldsymbol{\varepsilon}^{i\mathrm{e}}_{\text{int pt}}$ is the elastic strain vector of load step i at the most highly stressed integration point, calculated using the current stress vector and the linear elastic material model as follows:

$$\boldsymbol{\varepsilon}^{i\mathrm{e}}_{\text{int pt}} = \mathbf{C}\boldsymbol{\sigma}^{i}_{\text{int pt}} = \frac{1}{E}\begin{bmatrix} 1 & -v & 0 \\ -v & 1 & 0 \\ 0 & 0 & 2(1+v) \end{bmatrix}\boldsymbol{\sigma}^{i}_{\text{int pt}} \tag{15}$$

where $\mathbf{C}$ is the linear compliance matrix of 2D plane stress, for example, $\boldsymbol{\sigma}^{i}_{\text{int pt}}$ is the stress vector of load step i at the most highly stressed integration point.

The effective plastic strain $\varepsilon^{i\mathrm{p}}_{\mathrm{e}}$ is calculated, at the most highly stressed integration point, using Eq. (10) and paired with the corresponding effective stress σ^{i}_{e}, for each load step i:

$$\begin{aligned} &\Delta\boldsymbol{\varepsilon}^{i\mathrm{p}}_{\text{int pt}} = \boldsymbol{\varepsilon}^{i\mathrm{p}}_{\text{int pt}} - \boldsymbol{\varepsilon}^{(i-1)\mathrm{p}}_{\text{int pt}}, \quad \Delta\varepsilon^{i\mathrm{p}}_{\mathrm{e}} = \sqrt{\frac{2}{3}\Delta\boldsymbol{\varepsilon}^{i\mathrm{p}}_{\text{int pt}}\cdot\Delta\boldsymbol{\varepsilon}^{i\mathrm{p}}_{\text{int pt}}}, \\ &\varepsilon^{i\mathrm{p}}_{\mathrm{e}} = \varepsilon^{(i-1)\mathrm{p}}_{\mathrm{e}} + \Delta\varepsilon^{i\mathrm{p}}_{\mathrm{e}} \end{aligned} \tag{16}$$

At the end of performing this to all load increments, a complete universal curve of the effective stress σ^{i}_{e} and effective plastic strain $\varepsilon^{i\mathrm{p}}_{\mathrm{e}}$ is stored along with the $\boldsymbol{\sigma}^{i}_{\text{int pt}}$ and $\boldsymbol{\varepsilon}^{i}_{\text{int pt}}$ vectors as the improved material model. This marks the end of an analysis pass and prepares the algorithm for the coming passes if the displacement error, at the monitoring points, is not less than a specified tolerance. This preparation is in terms of using the improved universal curve to build the tangent element stiffness matrix for the following analysis pass. The first two terms of Eq. (12) are already established using the first load increment. The third term, plastic part, requires the estimation of the hardening modulus H^{i}_{j} at different levels of the effective stress $\sigma^{i-1}_{\mathrm{e}j}$ at integration point j. The deviatoric stress vector $\mathbf{S}^{i-1}_{j}$ and the effective stress level $\sigma^{i-1}_{\mathrm{e}j}$ are known since they are obtained from their accumulated values of the previous load step. The modulus H^{i}_{j} is evaluated using the current improved universal curve as follows, see Fig. 4:

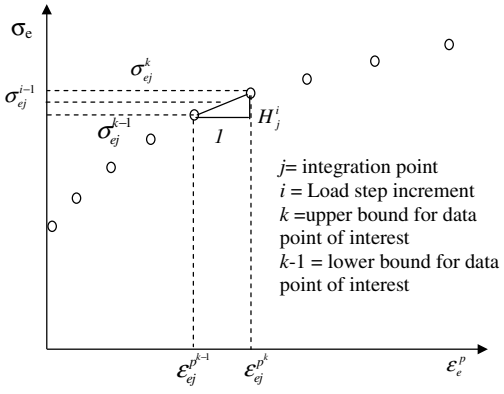

Fig. 4. Determination of the hardening modulus H using $\sigma_{\mathrm{e}} - \varepsilon^{\mathrm{p}}_{\mathrm{e}}$ data set of the most highly stressed integration point.

$$H_j^i = \frac{\sigma_{ej}^k - \sigma_{ej}^{k-1}}{\varepsilon_{ej}^{p^k} - \varepsilon_{ej}^{p^{k-1}}} \quad \text{and} \quad \sigma_{ej}^{k-1} < \sigma_{ej}^{i-1} < \sigma_{ej}^k, \quad \varepsilon_{ej}^{p^{k-1}} < \varepsilon_{ej}^{p^{i-1}} < \varepsilon_{ej}^{p^k} \tag{17}$$

where H_j^i is the modulus at load step i and integration point j needed to apply in Eq. (12). σ_{ej}^k and σ_{ej}^{k-1} are the two effective stress upper and lower bounds, from the universal curve, of the current stress level at integration point j, Fig. 4, $\varepsilon_{ej}^{p^k}$ and $\varepsilon_{ej}^{p^{k-1}}$ are the two effective plastic strain upper and lower bounds, from the universal curve, of the current strain level at integration point j, Fig. 4. Once is evaluated for each load increment i and integration point j, the tangent constitutive matrix, Eq. (13), is computed everywhere in the mesh and the tangent stiffness matrix, at each load step, is assembled.

$$\mathbf{K}_t^i = \int_{vol} \mathbf{B}_j^T \mathbf{D}_{tj}^{ep} \mathbf{B}_j \, dv \tag{18}$$

6. Applications

The following paragraphs explain four different examples for J2 plasticity model extraction using the current approach. The measured global response, at specific monitoring points, is obtained from standard forward nonlinear finite element analysis, with an analytical constitutive model. The effective stress–strain data corresponds to a universal curve expressed in terms of Ramberg–Osgood function and is used to generate the nonlinear response in the forward analysis. This function relates the effective stress (σ_e) to a total strain (ε) composed of an elastic strain and the effective plastic strain:

$$\varepsilon = \frac{\sigma_e}{E} + \varepsilon_e^p = \frac{\sigma_e}{E}\left[1 + \beta\left(\frac{\sigma_e}{\sigma_y}\right)^{n-1}\right] \Rightarrow \varepsilon_e^p = \frac{\beta\sigma_y}{E}\left(\frac{\sigma_e}{\sigma_y}\right)^n \Rightarrow \frac{1}{H} = \frac{d\varepsilon_e^p}{d\sigma_e} = \frac{n\beta}{E}\left(\frac{\sigma_e}{\sigma_y}\right)^{n-1} \tag{19}$$

Then, the present inverse approach is applied assuming that the material model is unknown a priori with the objective of extracting it back by matching the measured load–displacement curve, at the monitoring points, with the predicted one in each analysis pass. The code uses Q8 isoparametric plane stress finite elements. The general geometry of the problem, element numbering and element node numbering as well as integration point numbering for a master element are shown in Fig. 10. Different loading patterns are used for the purpose of examining all possible stress variations.

First, the process requires finding the linear material parameters for the first load increment, as discussed earlier. Then, the linear material model is used as an initial estimate for the finite element procedure to begin

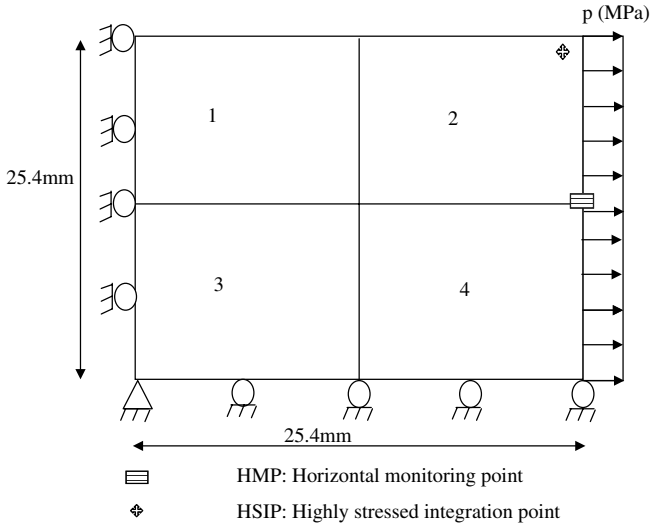

Fig. 5. Example 1, a simple uniaxial tension case.

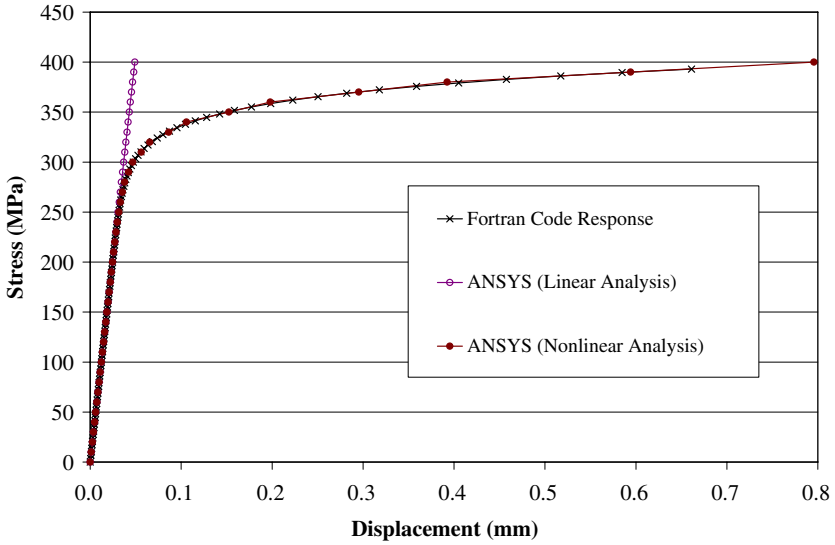

Fig. 6. Benchmarking for Example 1, simple uniaxial tension.

the inverse prediction. The examples shown here are chosen so that they reflect increasing level of complexity in the stress variation throughout the FE mesh. All the nonlinear load–displacement curves at the monitoring points are generated from a 2D nonlinear finite element FORTRAN program in forward analysis mode. The results of this program are benchmarked against ANSYS for the first example.

Example 1. (Simple uniaxial tension). This example is considered as the first step to demonstrating the performance of the present approach in predicting the J2 plasticity model. It consists of four elements composing a plate under uniaxial tension. The geometry, loading and boundary conditions are shown in Fig. 5. The plate has a thickness of 1 mm. The material model used to generate the actual load–displacement curve at the monitoring points in forward analysis is expressed in terms of a Ramberg–Osgood function given by the following equation:

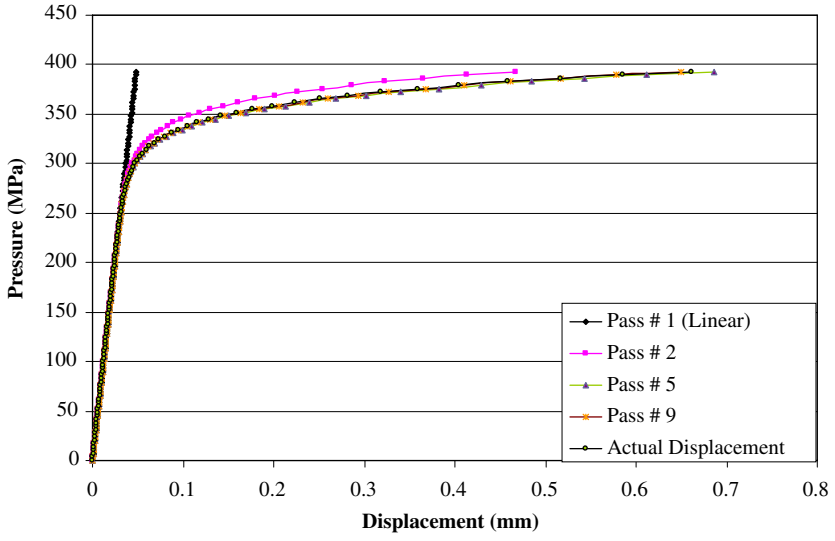

Fig. 7. Pressure–displacement curves for Example 1, simple uniaxial tension.

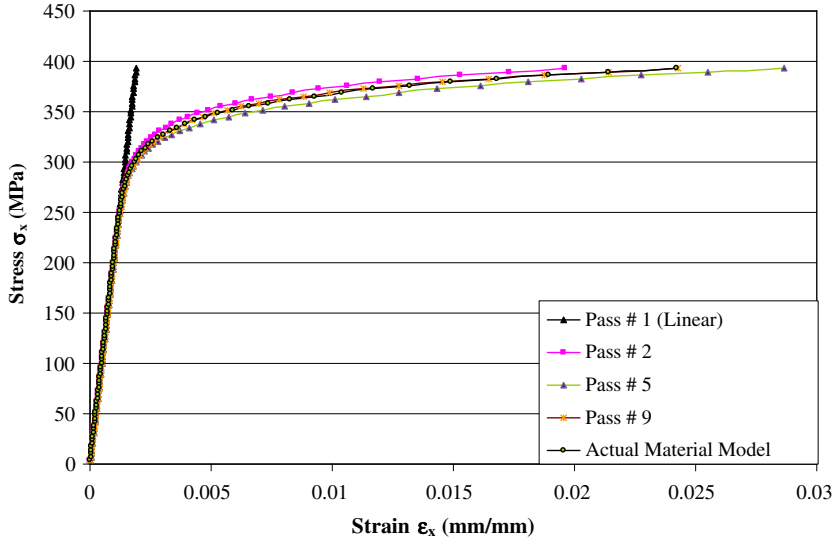

Fig. 8. Extraction of material model for Example 1, simple uniaxial tension.

$$\varepsilon = \frac{\sigma}{E}\left[1 + \frac{3}{7}\left(\frac{\sigma}{\sigma_y}\right)^{n-1}\right] \tag{20}$$

where $E =$ modulus of elasticity of the material $= 206{,}842$ MPa, $n =$ the material hardening coefficient $= 15$ and $\sigma_y = 0.2\%$ yielding stress $= 310$ MPa. In addition to the parameters of Eq. (20), the effective stress at initial deviation from linearity $\boldsymbol{\sigma}_o = 138$ MPa is given as it is needed in the forward plasticity analysis. The material assumed in this example is mild steel. To benchmark the results of this example, a comparison between the present analysis and that of ANSYS is presented in Fig. 6. Since the plate is under uniaxial tension, all nodes on the loaded edge experience the same displacement. One monitoring point at the middle of the loaded edge was enough to monitor displacements, Fig. 5. This selection is based on the maximum horizontal displacement location. Moreover, all integration points are under the same stress level. The most highly stressed integration point is taken as the integration point #9 for element #2, which is representative of any other point in the mesh. The progressive prediction of the load–displacement response at the selected monitoring point is shown

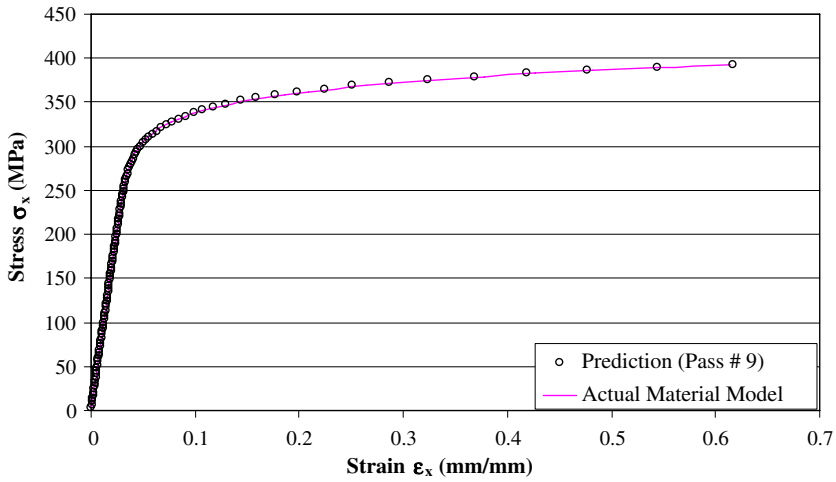

Fig. 9. Predicted material model for Example 1, simple uniaxial tension.

in Fig. 7. The improved prediction of the material model using the present approach is illustrated in Fig. 8, which shows such predictions for a number of passes on the way to completely capturing the actual material response. This inverse analysis required 9 passes to predict the material model very accurately, Fig. 9. However, it is evident that the solution from the second pass came very close to the actual one. This example shows that the present approach successfully works for simple load cases. Therefore, it is important to examine its applicability in recovering the local constitutive model for problems of more complex stress fields.

Example 2. (Biaxial tension) The second example examines the applicability of the present procedure with simple multi-axial stress states. It consists of a plate subjected to biaxial tension loading. This loading type does not involve shear stresses or strains. However, the two normal stress components are present. The material model used to generate the load–displacement response for the two selected monitoring points is Ramberg–Osgood with the following properties: $E = 60{,}000$ MPa, $\sigma_y = 60$ MPa and $n = 15$. In addition, the effective stress at initial deviation from linearity $\boldsymbol{\sigma}_o = 20$ MPa is needed in the forward plasticity analysis. These properties are assumed for an Aluminum Alloy. The dimension of the plate, mesh and loading are

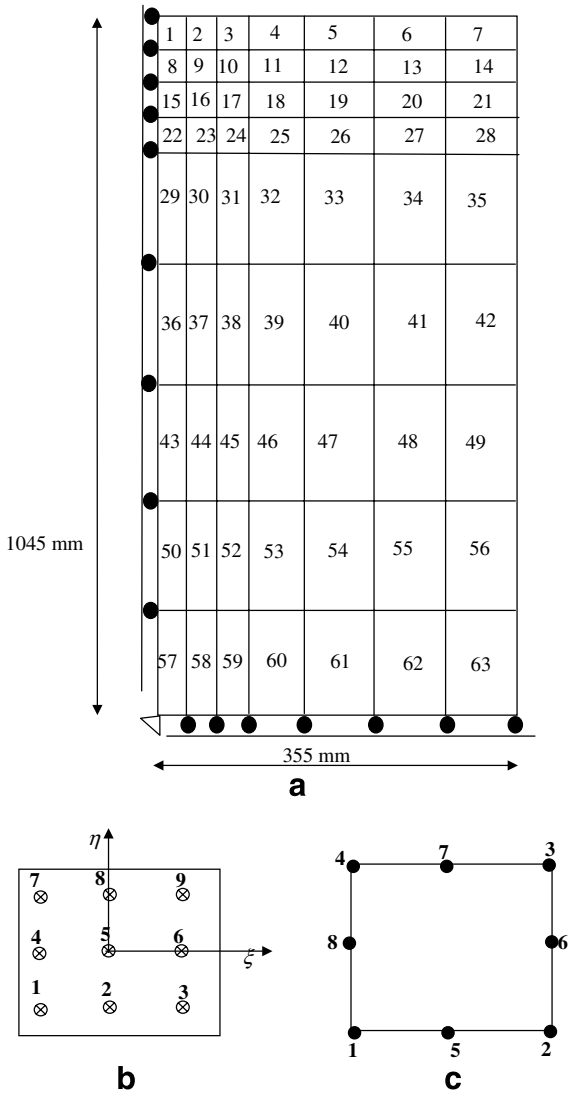

Fig. 10. (a) General geometry of the problem and element numbering. (b) Numbering of integration points in the master element. (c) Master element node numbering.

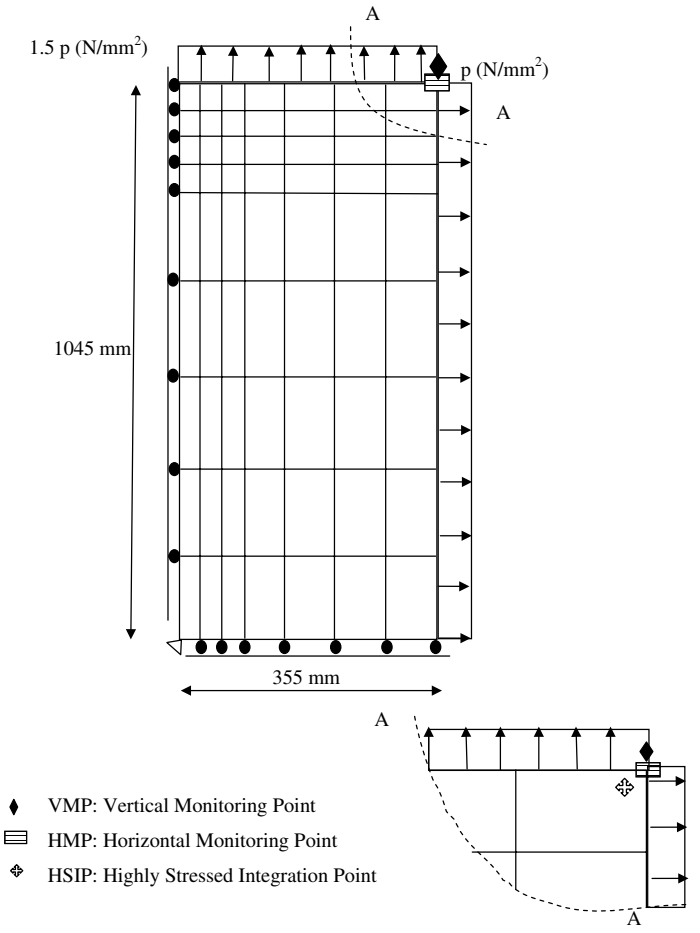

Fig. 11. Example 2, biaxial tension.

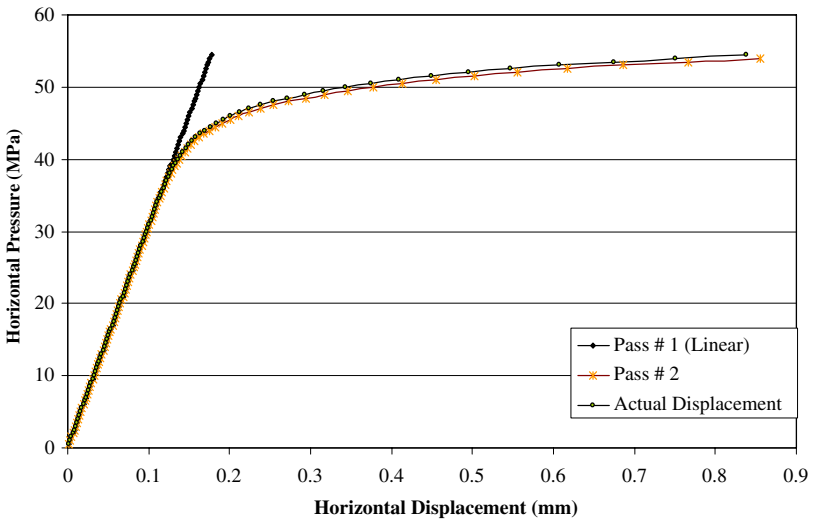

Fig. 12. Horizontal pressure–displacement prediction of Example 2, biaxial tension.

shown in Figs. 10 and 11. The plate has a thickness of 1 mm. Based on the location of maximum horizontal and vertical displacement, one monitoring point with two degrees of freedom are selected. Their load–displacement curves are obtained from forward analysis and used by the inverse analysis. These points are node #3 of element #7 for both vertical and horizontal displacement, Figs. 10 and 11. The most highly stressed integration point is also shown in Fig. 11 to be integration point #9 for element #7. After performing two passes, the predicted load–displacement curves, at the monitoring points, converged to the actual load–displacement response obtained from forward analysis. The progressive prediction of the horizontal and vertical load–displacement response is shown in Figs. 12 and 13, respectively. This is reflected onto an adaptively accurate prediction of the stress–strain curve at the most highly stressed integration point, Figs. 14 and 15. The effective stress–strain data correspond to the universal Ramberg–Osgood curve used to generate the nonlinear response in forward analysis. This relates the effective stress (σ_e) to the total strain (ε) composed of an elastic strain (σ_e/E) and the effective plastic strain (ε_e^p). The excellent comparison between the prediction and the actual material response proves the applicability of the present inverse J2 plasticity approach for simple multi-axial stress states. However, the two nonlinear examples presented so far have uniform stress fields with zero shear stresses. Therefore, the next two examples treat cases with variable stress states throughout the mesh.

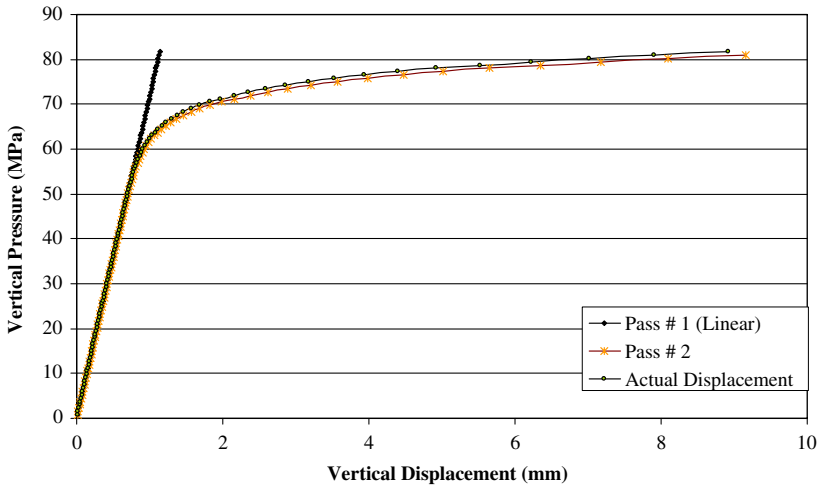

Fig. 13. Vertical pressure–displacement prediction of Example 2, biaxial tension.

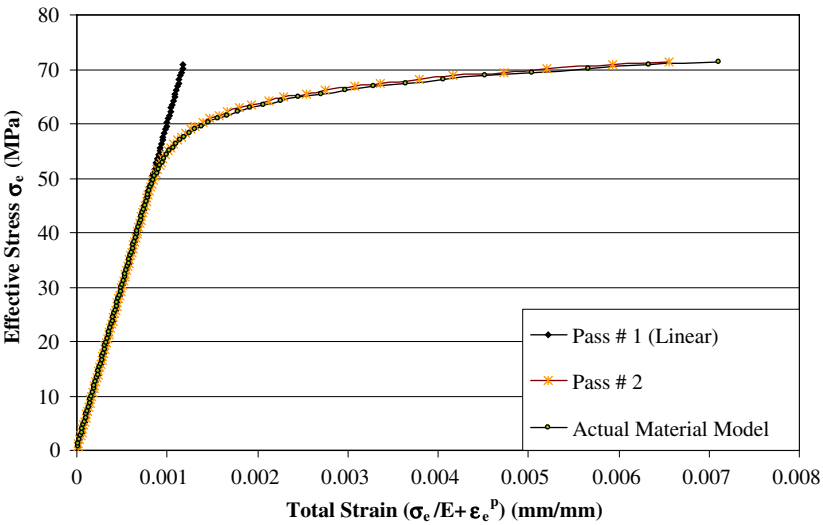

Fig. 14. Extraction of material model in Example 2, biaxial tension.

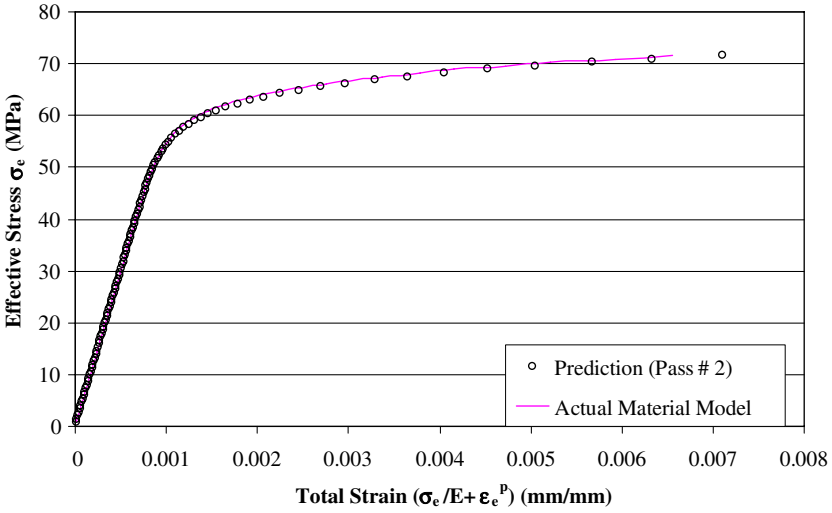

Fig. 15. Predicted vs. actual material model for Example 2, biaxial tension.

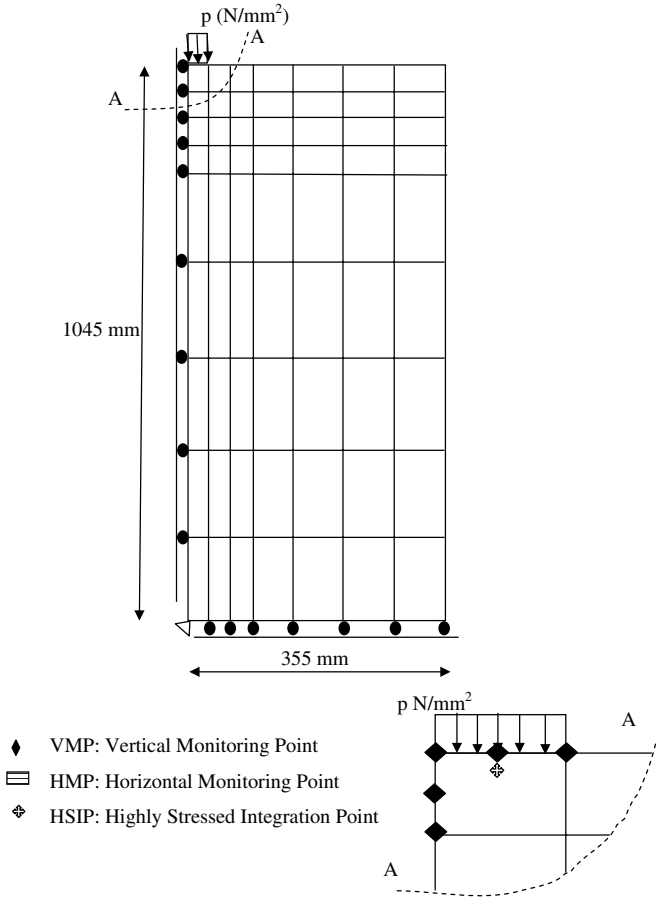

Fig. 16. Example 3, concentrated loading case.

Example 3. (The concentrated loading case) In this example, the plate is subjected to a simulated concentrated load causing its upper left part to be heavily stressed, Fig. 16. A J2 plasticity model is used in forward analysis to generate the load–displacement response at the chosen monitoring points. This material model has the same Ramberg–Osgood parameters used in the biaxial loading case analyzed in Example 2. The plate has a thickness of 1 mm as well. The monitoring points are placed in the vicinity of the highly stressed region and wherever maximum vertical displacements are computed, Fig. 16. The locations are at the 4th, 7th, 3rd, 8th and 1st nodes of element #1, Figs. 10 and 16. The most highly stressed integration point is #8 of element #1, Figs. 10 and 16. The present approach required six passes to converge to the correct nonlinear material model. The complete load–displacement curves for two selected monitoring points are shown in Figs. 17 and 18. It is worth to mention that the load–displacement curves predicted at pass #6 were almost same as the ones generated at passes #4 and #5. This gave the indication that these were the best load–displacement curves that could be predicted using the present approach and no more passes were needed. This is evident in Fig. 19 that

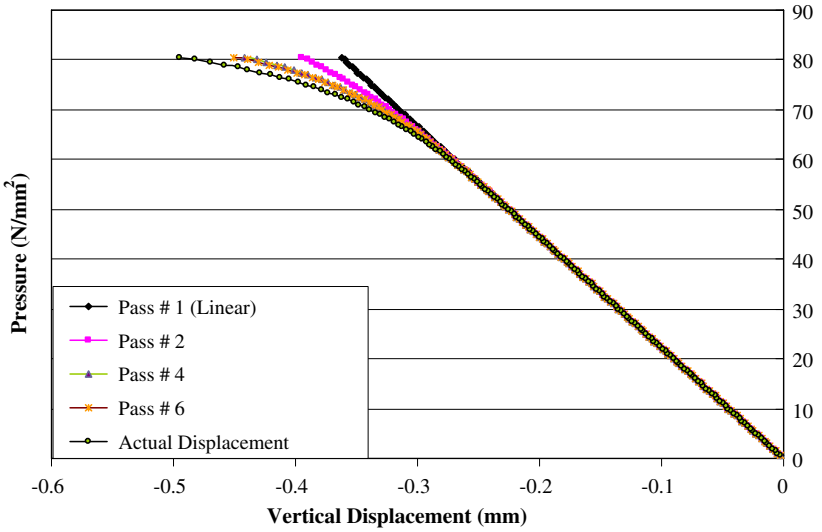

Fig. 17. Pressure–displacement prediction of 4th node of element 1 (Example 3).

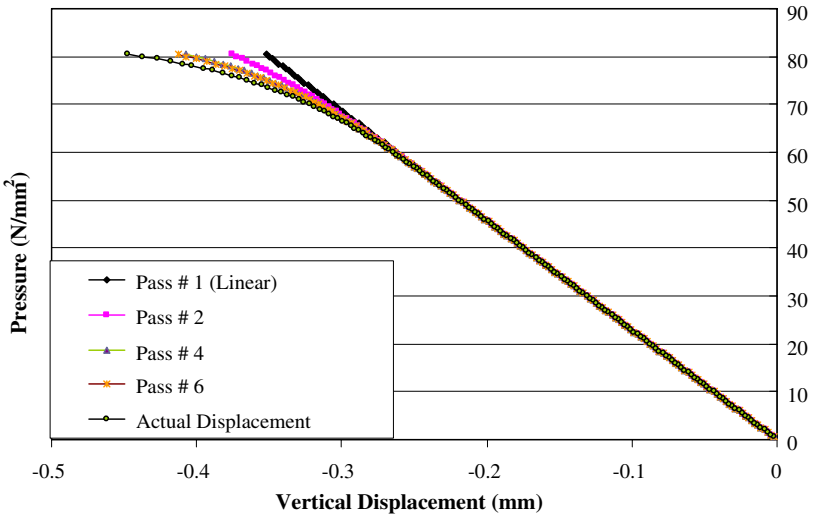

Fig. 18. Pressure–displacement prediction of 7th node of element 1 (Example 3).

shows the improvement of the material model prediction after each pass until convergence. Fig. 20, on the other hand, presents the latest material model of pass #6 compared to the actual material response. It can be clearly seen from these figures that the present approach successfully extracted the inherent material model from the global structural response despite the fact that the latter was not exactly matched. The effective stress–strain data corresponding to the universal Ramberg–Osgood curve is used to generate the nonlinear structural response in forward analysis. This relates the effective stress (σ_e) to the total strain (ε) composed of an elastic strain (σ_e/E) and the effective plastic strain (ε_e^p). The small discrepancy between the last predicted load–displacement curves and the actual ones could be attributed to the fact that the load–displacement response is an integration of the stress–strain curve throughout the mesh. Upon the start of yielding, few integration points show softer local response whereas the rest of the mesh is still in linear range. This may not be

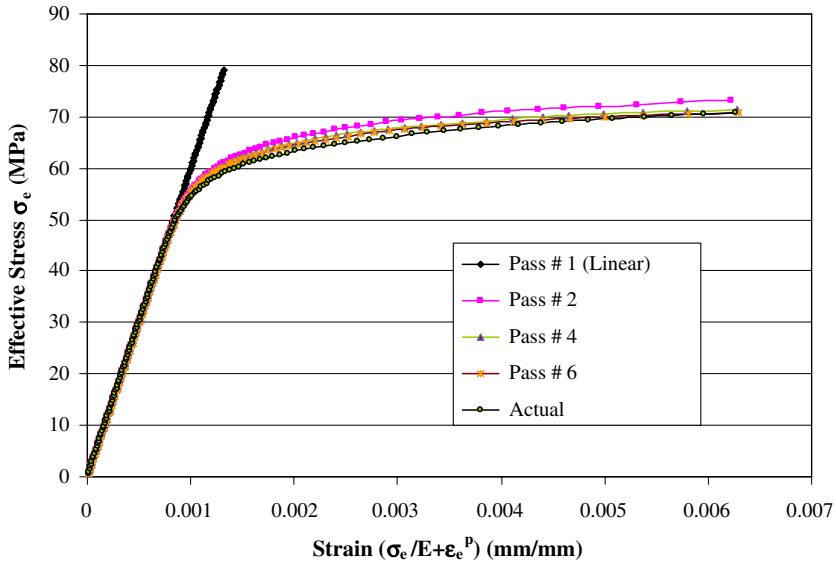

Fig. 19. Improved prediction of the material model for Example 3.

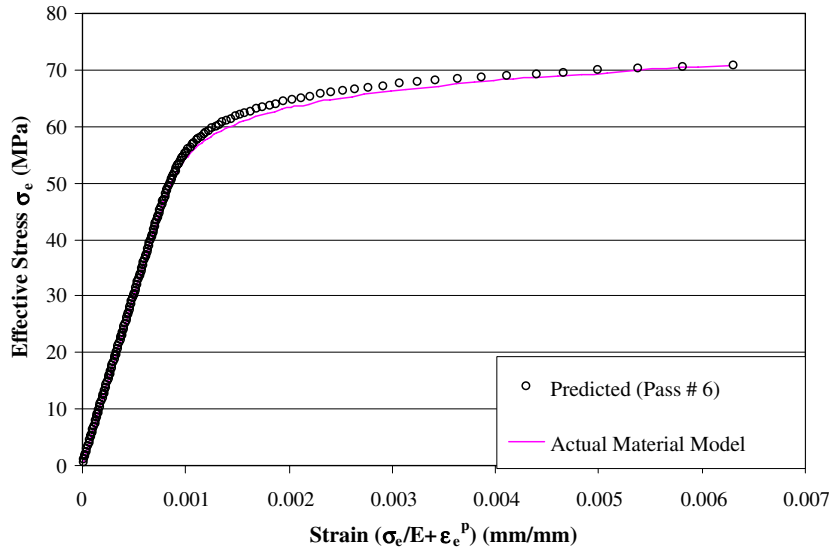

Fig. 20. Predicted vs. actual material model for Example 3.

clearly reflected on the load–displacement response at that load step. As the load increases, however, more integration points experience yielding and consequently nonlinearity becomes more pronounced. Accordingly, the selection of the most highly stressed integration point to recover the material model, from inverse analysis, allows it to detect and reflect the nonlinearity as it takes place.

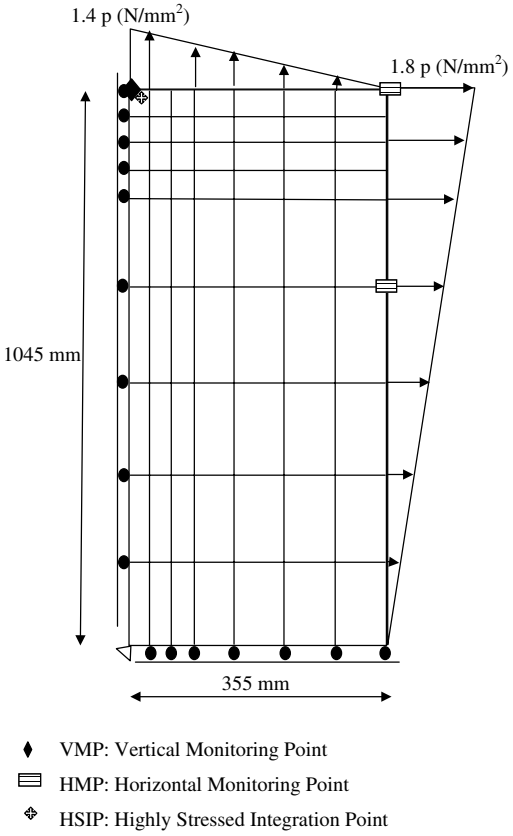

Fig. 21. Example 4, linearly varying edge loads.

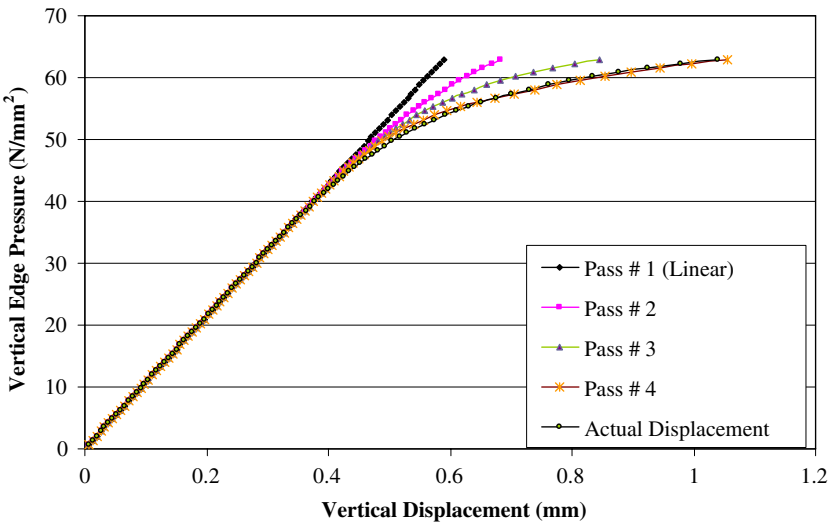

Fig. 22. Vertical pressure–vertical displacement prediction of Example 4, linearly varying edge loads.

Example 4. (Linearly varying edge loads) In this example, the same plate analyzed earlier is subjected to linearly varying loads on both of its sides. This causes the integration points to have gradual stress variation and, accordingly, forces more integration point into the yielding stage simultaneously. The material model, used in the forward analysis, is the same one used in Examples 2 and 3. The geometry, mesh and loading are shown in Fig. 21. The plate also has a thickness of 1 mm. Three monitoring points are selected as shown in Fig. 21. The selection is generally based on the location of the maximum displacements. Vertical displacement of the 4th node of element #1, horizontal displacement of the 3rd node of element #7 and mid height horizontal displacement of 2nd node of element # 35 are selected as monitoring locations. The most highly stressed integration point is #8 of element #1, Figs. 10 and 21. The load–displacement curve of the vertical monitoring point

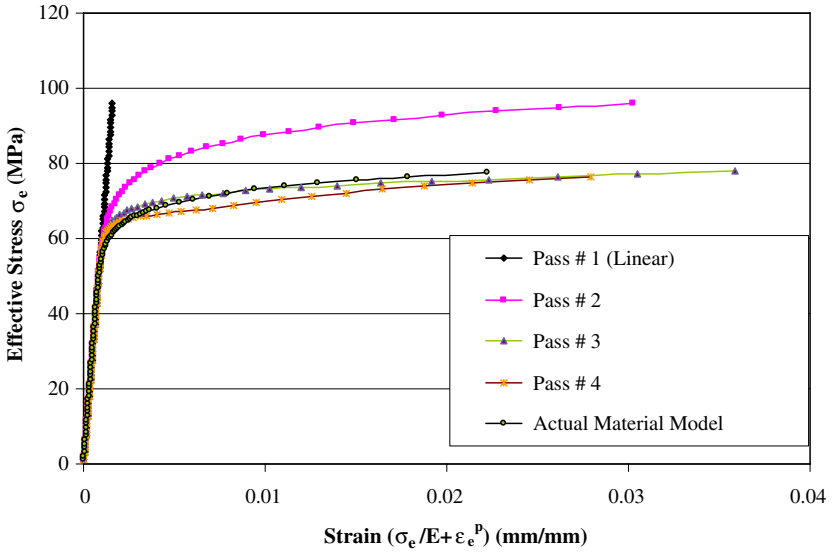

Fig. 23. Improved prediction of material model for Example 4, linearly varying edge loads.

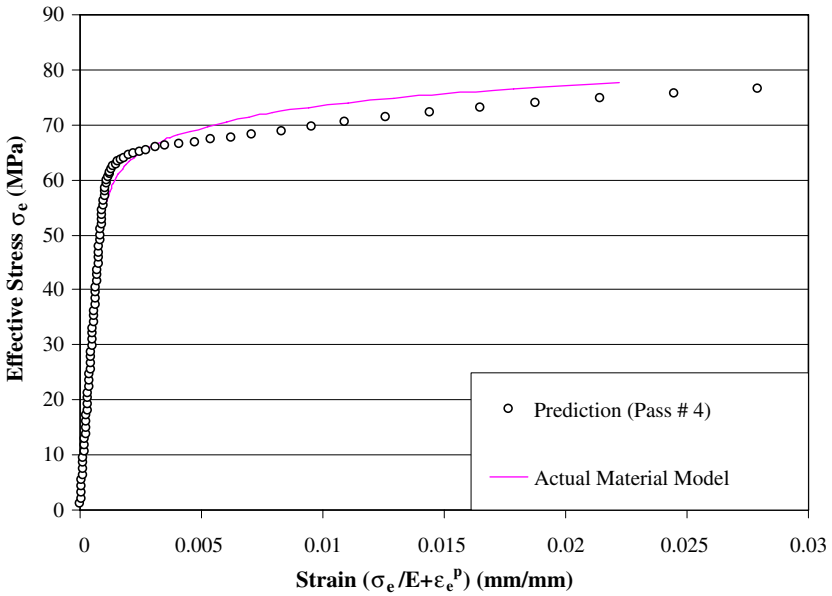

Fig. 24. Predicted vs. actual material model for Example 4, linearly varying edge loads.

shows that the predicted displacements match the actual displacements after four passes, Fig. 22. The progressive improvement of the material model is presented in Fig. 23. The prediction of the material model is seen to be in close agreement with the actual curve, Fig. 24. The effective stress–strain data corresponding to the universal Ramberg–Osgood curve is used to generate the nonlinear structural response in forward analysis. This relates the effective stress (σ_e) to the total strain (ε) composed of an elastic strain (σ_e/E) and the effective plastic strain (ε_e^p). It is important to note that the prediction of the load–displacement curves at the monitoring points using the improved material model after each pass does not require any check for yielding. The softening in the plate stiffness is naturally captured from the material model data extracted from the stress–strain profile of the most highly stressed integration point through Eq. (17).

7. Conclusions

In this paper, the use of global response to inversely calibrate accurate J2 universal curve has been treated. The present approach provides explicit, robust, and computationally efficient way to recover local constitutive behavior by focusing on the results of the most highly stressed integration point. Rational formulation of the stiffness matrix based on a J2 plasticity framework is presented. The approach is general and it could be extended to other nonlinear material models and boundary value problems. The examples solved show great potential of the present approach to be used in conjunction with non-contact displacement measurement techniques like digital image correlation. Generally speaking, the more the data provided to the inverse algorithm the better and faster the material model extraction. However, it is evident that the strategic location of monitoring points helps attain accurate and efficient predictions. It is recommended to perform a linear finite element analysis using any arbitrary material model to identify the location of maximum displacements and the most highly stressed integration point. Placing the monitoring points at the locations of maximum displacement is found to greatly facilitate convergence. It is important to note that earlier studies did not address the relationship between the number and location of monitoring points and the complexity of the stress field. It is also important to mention that existing noise in measured data may negatively impact the convergence of the present algorithm. Accordingly, smoothing of the measured data should be used prior to implementing the data in the present procedure. This smoothing may be performed using a one time neural network or least square fitting of data.

Acknowledgments

The authors like to acknowledge the support of the National Science Foundation through its Grant NSF-CMS0334391 and the additional support of the Department of Civil Engineering at Kansas State University.

References

Forestier, R., Massoni, E., Chastel, Y., 2002. Estimation of constitutive parameters using an inverse method coupled to a 3D finite element software. Journal of Material Processing Technology 125–126, 594–601.

Furukawa, T., Sugata, T., Yoshimora, S., Hoffman, M., 2002. An automated system for simulation and parameter identification of inelastic constitutive models. Computer Methods in Applied Mechanics and Engineering 191, 2235–2260.

Gelin, J.C., Ghouati, O., 1995. Inverse approach for the determination of constitutive equations in metal forming. CIRP Annals-Manufacturing Technology 44 (1), 189–192.

Ghaboussi, J., Pecknold, D., Zhang, M., Haj-Ali, R., 1998. Auto-progressive training of neural network constitutive models. International Journal for Numerical Methods in Engineering 42, 105–126.

Lam, Y.C., Khoddam, S., Thomson, P.F., 1998. Inverse computational method for constitutive parameters obtained from torsion, plane-strain and axisymmetric compression tests. Journal of Material Processing Technology 83 (1–3), 62–71.

Liu, S.W., Huang, J.H., Sung, J.C., Lee, C.C., 2002. Detection of cracks using neural networks and computational mechanics. Computer Methods in Applied Mechanics and Engineering 191 (25–26), 2831–2845.

Li, J., Chen, J., 2000. Structural parameters identification with unknown input. Computing in Civil and Building Engineering 1, 287–293.

Markiewicz, E., Ducrocq, P., Drazetic, P., 1998. Inverse approach to determine the constitutive model parameters from axial crushing of thin-walled square tubes. International Journal of Impact Engineering 21 (6), 433–449.

Nayal, R., Rasheed, H.A., 2006. Tension stiffening model for concrete beams reinforced with steel and FRP bars. Journal of Materials in Civil Engineering, ASCE 18 (6), 831–841.

Ohkami, T., Swoboda, G., 1999. Parameter identification of viscoelastic material. Computers and Geotechnics 24 (4), 279–295.
Rikards, R., Chate, A., Gailis, G., 2001. Identification of elastic properties of laminates based on experimental design. International Journal of Solids and Structures 38 (30–31), 5097–5115.
Sakurai, T.K., 1983. Back analysis of measured displacement of tunnels. Journal of Rock Mechanics and Rock Engineering 16 (173), 173–180.
Shin, H.S., Pande, G.N., 2000. On self-learning finite element codes based on monitored response of structures. Computers and Geotechnics 27 (3), 161–178.
Shin, H.S., Pande, G.N., 2003. Identification of elastic constants for orthotropic materials from structural test. Computers and Geotechnics 30 (7), 571–577.
Soh, C.K., Dong, Y.X., 2001. Evolutionary programming for inverse problems in civil engineering. Journal of Computing in Civil Engineering 15 (2), 144–150.